

## A UNIFIED DYNAMIC SIMILITUDE OF SOLID CONTINUUM AND ITS APPLICATION IN AEROELASTIC STRUCTURES

Oluwamayokun B. Adetoro<sup>1</sup>, Thomas B. Goonan<sup>1</sup> and Rui P.R. Cardoso<sup>1</sup>

<sup>1</sup> Department of Mechanical and Aerospace Engineering,  
Brunel University London, UB8 3PH  
Uxbridge, London, UK.  
Mayo.Adetoro@brunel.ac.uk  
Thomas.Goonan2@brunel.ac.uk  
Rui.Carodos@brunel.ac.uk

**Keywords:** aeroelastic scaling, scaling laws, dynamic similitude, fluid-structure interaction, computational fluid dynamics, computational structural dynamics.

**Abstract:** The use of dynamic similitude has been widely proven in fluid mechanics. With the drive for efficient aircraft wing through high aspect ratio wings comes the growing need for much more accurate aeroelastic analyses of aircraft wings and more accurate scaled experimental tests. Even with this need for dynamic similitude in solid mechanics, there is still no unified exact scaling law applicable to any given solid structure or system. Here we present a recently proposed unified similitude model for solid mechanics using the momentum and the energy conservation. The model allows for the use of different materials in both elastic and plastic regimes. Never reported dimensionless numbers are derived for the first time in this article, and this set of numbers is sufficient for strictly accurate dynamic similitude of any solid structure. The application of the unified model is demonstrated for the first time in an aeroelastic structure and in aerospace structures through case studies. The very good agreement seen in compared results confirms the accuracy of the developed scaling model and the exactness of the dimensionless numbers.

### 1 INTRODUCTION

Our theories and understanding are based on direct observations of the phenomena in question, observations which produce solutions to immediate practical problems. However, there are times when engineers and scientists are interested in or only find it feasible to make observations in a scale replica (hereafter called the “model”) of a full-scale artefact or phenomena (hereafter called the “prototype”). The success of the design and analysis of a new engineering system (e.g. a wing box structure) is broadly dependent on many investigations conducted through theoretical, computational and experimental verifications. However, if the (new) system is complex enough that there is the lack of a scientific model to predict its behaviour, extensive experimental evaluation is often used until a deep understanding is attained. For large and oversized systems, creating the actual working conditions for testing the prototype can be very expensive, time-consuming or impossible. Such a situation is prevalent in the design and analysis of aeroelastic structures. A desired viable alternative is the experimental observation on a “dynamically similar” model and the subsequent scaling of measurements back to the solutions applicable to the prototype. Following the design and

analysis stages of new aircraft structure designs, the necessary aeroelastic certification process also requires the validation of the design and numerical modelling results through a series of experimental tests. Jonathan et al. [1] listed the series of tests that must be performed in order to satisfy airworthiness regulations relating to aeroelasticity.

Newton was among the first to articulate the idea of similitude when he considered the similarity in the motion of bodies in his famous Principia [2]. He also made mention of the similar motion (kinematic similitude) and proportional times (temporal similitude) of similar bodies or systems in like situations. This similar motion by similar systems was explored by Stokes immediately after he developed the equations for calculating the motion of a fluid. He discussed the conditions for dynamic similitude in similar systems with different or the same fluid [3]. With this foundation laid in fluid dynamics, the importance of dynamic similitude in fluid dynamics has grown since Reynolds presented his factor, which determines the character of fluid motion [4]. Later on, Rayleigh broadly discussed several scientific models and factors based on similitude [5]. For fluid continua, attaining dynamic similarity between two different continuums is well established and attainable with the use of relevant dimensionless parameters.

For solid mechanics, on the other hand, there have been several attempts at attaining similitude. Most of these have resulted in some form of similitude model or the other, which are problem and case-specific. Still, all have failed in offering a unified approach to dynamic similitude in solid mechanics. Goodier and Thomson [6] were probably the first to extensively explore the application of similitude to structures, although their work was for systems in static equilibrium. After this study, the interest for scaled structural problems has been seen in several applications, including space vehicles [7], solar sail systems [8], shipping casks [9], marine structures [10], flat plates [11], composite structures [12], a gantry crane [13] and an aircraft fuselage [14]. A more in-depth review of past studies has been conducted in several publications in the literature [15-18].

In the scaling of aeroelastic structures, there has been very limited progress, even though it plays a vital role in studying the aeroelastic characteristics of full-size aircraft. Bisplinghoff [19] presented the classical approach to aeroelastic scaling, which is only applicable to linear structures. The following studies have attempted to tackle the effect of geometric non-linearity [20-23] and presented the scaling of typical aeroelastic section models. The optimisation approach to aeroelastic scaling has also been presented by [24-27]. The optimisation seeks to minimise the difference in scaled static deflections between deflections and differences in mode shapes. A detailed review of aeroelastic scaling was presented by Afonso [28]. Whilst satisfactory similarity of aeroelastic structures has been demonstrated in some past work, there is still the lack of a unified approach to achieving exact similitude.

Past studies on dynamic similitude, especially for solid or aeroelastic structures, have intrinsically been unable to arrive at a unified model because the studies have been using either Buckingham Pi's theorem or using some governing equations of motion or equilibrium equations that are unique to the particular system in question, while others have used modal analyses and even empirical approaches to obtain scaling factors. This lack of a unified scaling model in solid mechanics has led to the varied approaches for attaining dynamic similitude in solid continuum reported in the literature. The Buckingham Pi's theorem [29], a remarkable theorem, has undoubtedly underpinned most of the past work carried out in dynamic similitude. It gives valuable insight into a given problem without the reliance on complex governing laws. Apart from producing problem-specific results, another weakness of the Buckingham Pi approach is that it requires the prior knowledge or selection of all the dimensioned variables

(so-called Pi groups) that influence the behaviour of the dynamical system and its success relies heavily on the accurate selection of these variables. Governing equations of motion are not always readily available for a given system; however, when used, they always result in a solution for a dynamically similar system. This trend for problem-specific scaling model remains prevalent in the literature as seen by some of the most recent studies, such as the study by Li et al. [30] in which a partial similitude method was proposed, or the study by El-Borgi et al. [31] in which they used dynamic similitude to study the vibration of scaled piping systems, or the recent study by Afonso et al. [32] in which they used the Buckingham Pi's theorem to solve the scaling of a flexible high aspect-ratio wing using different strategies.

In the recent review article by Casaburo et al. [18], they categorised the different methods that exist in the literature, and they explored the increasing range of areas and disciplines in which dynamic similitude in solid mechanics is being attempted. This increase in the interest in dynamic similitude is partly due to the advantages a scaled model offers, especially in experimental tests performed for research, design, planning, validation, safety and certification purposes. The use of dynamic similitude will, however, only increase with improvements in non-destructive or non-contacting testing and the greater flexibility in the fabrication of parts offered by novel additive manufacturing processes. With stringent sustainability goals for the next generation of commercial transport aircraft, such designs as the ultra-high aspect-ratio wing configuration are seen as a key enabler and for which non-linear geometrical effects are much more profound. There is, therefore, the need for more accurate aeroelastic analysis of aircraft wings, more accurate experimental tests both at the design and certification stages of new aircraft and a unified model that achieves exact dynamic similitude in aeroelastic structures.

In this article, we present the very recent unified exact dynamic similitude model for solid continuum developed by Adetoro and Cardoso [33] and, for the first time, apply the model to aeroelastic structures. Geometric non-linearity is considered in the model, and the set of non-dimensional coefficients for achieving dynamic similarity in any dynamical systems using both the momentum and energy conservation are derived in this model and never reported dimensionless numbers are derived. The unified model is generic in that its use is not restricted to any particular structural problem; hence its application to aeroelastic structures is demonstrated. The solutions developed in this paper focus solely on purely mechanical processes, where heat sources and heat fluxes are ignored.

## 2 UNIFIED MODEL

The approach presented here is applicable to solid structures or systems for which the continuum assumption holds or structures for which a homogenised representative volume element can be defined. The momentum equation (balance of linear momentum) for such a structure is defined as,

$$\rho \frac{Du_i}{Dt} = \rho f_i + \frac{\partial \sigma_{ji}}{\partial x_j} \quad i, j = 1, 2, 3 \quad (1)$$

By obtaining the virtual work principle at a particular point in the domain of analysis and integrating over the whole domain, we can define the total virtual work as,

$$\int_V \rho \frac{Du_i}{Dt} \delta x_i \, dV = \int_V \left( \rho f_i + \frac{\partial \sigma_{ji}}{\partial x_j} \right) \delta x_i \, dV \quad (2)$$

where,  $\delta x_i$  are the generic virtual displacements along the rectangular axes of  $x_i$ ;  $u_i$  are the components of the velocity;  $f_i$  are the components of the body force per unit mass;  $t$  is time,  $\rho$  the density, respectively. By rearranging using product rule and by integrating the RHS of (2) by parts and given that,

$$\sigma_{ji} \frac{\partial \delta x_i}{\partial x_j} = \sigma_{ji} \left\{ \frac{1}{2} \left( \frac{\partial \delta x_i}{\partial x_j} + \frac{\partial \delta x_j}{\partial x_i} \right) \right\} = \sigma_{ij} \delta e_{ij}$$

we can derive the weak formulation as follows,

$$\int_V \rho \frac{Du_i}{Dt} \delta x_i dV = \int_V \rho f_i \delta x_i dV - \int_V \sigma_{ij} \delta e_{ij} dV + \int_\Gamma \sigma_{ji} \delta x_i n_j d\Gamma \quad (3)$$

where,  $n_j$  are the components of the shear plane's normal vector,  $V$  and  $\Gamma$  are respectively the domain volume and boundary,  $\sigma_{ij}$  and  $\delta e_{ij}$  are the Cauchy stress and strain, respectively.

The Cauchy stress tensor is defined at the current configuration, however (3) can be defined for a given continuous domain, and at any given time as,

$$\int_V \rho \frac{Du_i}{Dt} \delta x_i dV = \int_V \rho f_i \delta x_i dV - \int_V S_{ij} \delta \varepsilon_{ij} dV + \int_\Gamma T_i \delta x_i d\Gamma \quad (4)$$

where,  $T_i$  are the components of the stress vector at the boundary or surface force.  $S_{ij}$  and  $\varepsilon_{ij}$  are the second Piola-Kirchhoff stress tensor and the Green-Lagrange strain tensors, respectively; both defined in a co-rotational coordinate system at the reference configuration. By defining the displacement, strain and stresses in an incremental fashion, we have, for example, for an isotropic material,

$$\int_V \left( \rho \frac{\partial u_i}{\partial t} + \rho u_j \frac{\partial u_i}{\partial x_j} \right) \delta x_i dV = \int_V \rho f_i \delta x_i dV - \int_V \lambda C_{ijmn_1} \Delta \varepsilon_{mn}^l \delta \varepsilon_{ij}^l dV - \int_V 2\mu C_{ijmn_2} \Delta \varepsilon_{mn}^l \delta \varepsilon_{ij}^l dV - \int_V {}^{t+\Delta t} S_{ij} \delta \varepsilon_{ij}^{nl} dV - \int_V {}^{t+\Delta t} S_{ij} \delta \varepsilon_{ij}^l dV + \int_\Gamma T_i \delta x_i d\Gamma \quad (5)$$

where, subscripts  $m, n = 1, 2, 3$ ,  $\delta \varepsilon_{ij}^l$ ,  $\Delta \varepsilon_{ij}^l$  and  $\delta \varepsilon_{ij}^{nl}$ ,  $\Delta \varepsilon_{ij}^{nl}$  are the infinitesimal and incremental linear and non-linear parts of the strain tensor;  $\lambda$  and  $\mu$  are the first and second Lamé constants;  $C_{ijmn_1}$  and  $C_{ijmn_2}$  are the material stiffness matrices, respectively. Equations (5) can also be written for orthotropic materials.

For fluids continuum, Stokes [3] argued the unnecessary complexity in the complete determination of the time integrals of his equations similar to (5), since it would be necessary to put  $t = 0$  in the equations and equate the results to the initial velocities. It is often impossible and unnecessary to describe the motion of a fluid continuum with respect to initial conditions or a reference configuration since the behaviour of a Newtonian fluid is generally independent of its history. On the other hand, for solid continuum, the stresses generally depend on the history of deformation and the strain is defined in relation to the initial conditions because the behaviour of solids is history-dependent.

Therefore, obtaining a complete similitude solution for the phenomena in question (the prototype) calls for the integration of equations (5) over time. If we assume that the physical situation exists from a state of rest where initial velocities are zero, we can, using Leibniz's rule, define the first term in (5) as,

$$\int_V \rho \frac{\partial u_i}{\partial t} \delta x_i dV = \frac{d}{dt} \int_V \rho u_i \delta x_i dV - \left( \rho u_i \delta x_i \frac{\partial V}{\partial t} \right) \Big|_t \quad (6)$$

Therefore (5) becomes,

$$\begin{aligned} \frac{d}{dt} \int_V \rho u_i \delta x_i dV - \left( \rho u_i \delta x_i \frac{\partial V}{\partial t} \right) \Big|_t &= - \int_V \rho u_j \frac{\partial u_i}{\partial x_j} \delta x_i dV + \int_V \rho f_i \delta x_i dV - \\ &\int_V \lambda C_{ijmn_1} \Delta \varepsilon_{mn}^l \delta \varepsilon_{ij}^l dV - \int_V 2\mu C_{ijmn_2} \Delta \varepsilon_{mn}^l \delta \varepsilon_{ij}^l dV - \\ &\int_V {}^{t+\Delta t} S_{ij} \delta \varepsilon_{ij}^{nl} dV - \int_V {}^{t+\Delta t} S_{ij} \delta \varepsilon_{ij}^l dV + \int_{\Gamma} T_i \delta x_i d\Gamma \end{aligned} \quad (7)$$

We can integrate with respect to time, and we have,

$$\begin{aligned} \int_V \rho u_i \delta x_i dV - (\rho u_i V \delta x_i) \Big|_t &= - \int_V \int \rho u_j \frac{\partial u_i}{\partial x_j} \delta x_i dV dt + \int_V \int \rho f_i \delta x_i dV dt - \\ &\int_V \int \lambda C_{ijmn_1} \Delta \varepsilon_{mn}^l \delta \varepsilon_{ij}^l dV dt - \int_V \int 2\mu C_{ijmn_2} \Delta \varepsilon_{mn}^l \delta \varepsilon_{ij}^l dV dt - \\ &\int_V \int {}^{t+\Delta t} S_{ij} \delta \varepsilon_{ij}^{nl} dV dt - \int_V \int {}^{t+\Delta t} S_{ij} \delta \varepsilon_{ij}^l dV dt + \int F_i^{ext} \delta x_i dt \end{aligned} \quad (8)$$

where,  $F_i^{ext}$  are the components of the external force. By non-dimensionalising (8), we obtain,

$$\begin{aligned} \int_V \bar{\rho} \bar{u}_i \delta \bar{x}_i d\bar{V} - (\bar{\rho} \bar{u}_i V \delta \bar{x}_i) \Big|_{\bar{t}} &= - \int_V \int \bar{\rho} \bar{u}_j \frac{\partial \bar{u}_i}{\partial \bar{x}_j} \delta \bar{x}_i d\bar{V} d\bar{t} + \frac{f_{ref} L_{ref}}{u_{ref}^2} \int_V \int \bar{\rho} \bar{f}_i \delta \bar{x}_i d\bar{V} d\bar{t} - \\ &\frac{E_{ref}}{\rho_{ref} u_{ref}^2} \int_V \int \bar{\lambda} \bar{C}_{ijmn_1} \Delta \bar{\varepsilon}_{mn}^l \delta \bar{\varepsilon}_{ij}^l d\bar{V} d\bar{t} - \\ &\frac{E_{ref}}{\rho_{ref} u_{ref}^2} \int_V \int 2\bar{\mu} \bar{C}_{ijmn_2} \Delta \bar{\varepsilon}_{mn}^l \delta \bar{\varepsilon}_{ij}^l d\bar{V} d\bar{t} - \frac{E_{ref}}{\rho_{ref} u_{ref}^2} \int_V \int {}^{t+\Delta t} \bar{S}_{ij} \delta \bar{\varepsilon}_{ij}^{nl} d\bar{V} d\bar{t} - \\ &\frac{E_{ref}}{\rho_{ref} u_{ref}^2} \int_V \int {}^{t+\Delta t} \bar{S}_{ij} \delta \bar{\varepsilon}_{ij}^l d\bar{V} d\bar{t} + \frac{J_{ref}}{\rho_{ref} u_{ref} L_{ref}^3} \int \bar{F}_i^{ext} \delta \bar{x}_i d\bar{t} \end{aligned} \quad (9)$$

Therefore, we have the following first three coefficients from (9), and the fourth coefficient is obtained by non-dimensionalising (5),

$$\frac{f_{ref} L_{ref}}{u_{ref}^2}; \frac{E_{ref}}{\rho_{ref} u_{ref}^2}; \frac{J_{ref}}{\rho_{ref} u_{ref} L_{ref}^3}; \frac{T_{ref}}{\rho_{ref} u_{ref}^2} \quad (10)$$

where  $E_{ref}$  is the reference modulus of elasticity,  $J_{ref}$  is the characteristic impulse imposed at the boundary of the domain,

$$\begin{aligned} \bar{x}_i &= \frac{x_i}{L_{ref}}; \bar{u}_i = \frac{u_i}{u_{ref}}; \bar{\rho} = \frac{\rho}{\rho_{ref}}; \bar{t} = \frac{t}{t_{ref}}; \bar{V} = \frac{V}{L_{ref}^3}; \bar{f}_i = \frac{f_i}{f_{ref}}; \bar{\lambda} = \frac{\lambda}{E_{ref}}; \bar{\mu} = \frac{\mu}{E_{ref}}; \bar{S}_{ij} = \frac{S_{ij}}{E_{ref}}; \\ \bar{T}_i &= \frac{T_i}{T_{ref}} \end{aligned} \quad (11)$$

The reference values are characteristic values, and when selecting them, they must be representative, or they must quantify the dimensions or the respective variable in accordance with (9). When this is the case, then the coefficients in (10) will retain the characteristic dynamic behaviour of two independent systems (e.g. model and prototype), hence attain dynamic similarity.

The first coefficient in (10) is Froude's number, the second and fourth coefficients are analogous to Cauchy number and Johnson's damage number [34]. The second coefficient is the ratio between the elastic and the inertial force. The fourth coefficient is the ratio of applied surface force to the inertial force, and the third is a ratio of the externally applied impulse at the boundary to the characteristic momentum. To the best of the authors' knowledge, the third number is a ratio that has never been defined in the literature, and neither is it analogous to any existing number. In (9), we have equated the ratio of characteristic length to the characteristic time period as the characteristic velocity (i.e.  $u_{ref} = L_{ref} / t_{ref}$ ). In (9), the same coefficient is obtained for the linear and non-linear terms on the right-hand side; hence dynamic similarity is guaranteed for large deformations.

The coefficients in (10) are sufficient for achieving dynamic similitude for any given solid domain with varying material and any given spatial and temporal scales provided the continuum assumption remains valid. The coefficients also remain strictly accurate if the same material or if different materials are used. Adetoro and Cardoso [33] already dealt with dynamical structures when the domain deforms into the plastic region. The dynamically similar solutions obtained at any given time will always exist at the same strain state right through the evolution of deformation because the strain tensor in the domain defined by (8) is dimensionless and so cannot be scaled. This constraint is seen across different past studies.

It is possible, however, to still have dynamic similarity whilst enforcing the ratio of deformation to the characteristic length (i.e. strain) to be variable, which to date has not been possible. For this, we will consider the energy equation, which for purely mechanical processes in the continuum can be defined as,

$$\rho \frac{Dw^{int}}{Dt} = \sigma_{ij} \frac{\partial u_i}{\partial x_j} \quad i, j = 1, 2, 3 \quad (12)$$

where,  $w_{int}$  is the internal energy per unit mass. If we multiply (1) by the velocity vector,  $u_i$ , then add it to (12), and integrate over the entire domain, we obtain,

$$\int_V \rho \frac{Dw^{int}}{Dt} dV = \int_V \sigma_{ij} \frac{\partial u_i}{\partial x_j} dV - u_i \int_V \rho \frac{Du_i}{Dt} dV + u_i \int_V \rho f_i dV + u_i \int_V \frac{\partial \sigma_{ji}}{\partial x_j} dV \quad (13)$$

By using Cauchy's law and Gauss' theorem we have,

$$\int_V \left( \rho \frac{\partial w^{\text{int}}}{\partial t} + \rho u_j \frac{\partial w^{\text{int}}}{\partial x_j} \right) + \left( \frac{\rho}{2} \frac{\partial u_i^2}{\partial t} + \frac{\rho u_j}{2} \frac{\partial u_i^2}{\partial x_j} \right) dV = \int_V \rho f_i u_i dV + \int_{\Gamma} u_i T_i d\Gamma \quad (14)$$

Again, if we consider a physical situation that exists from a state of rest where initial internal energies and velocities are zero, we can, using Leibniz's rule, define the first two terms in (14) as,

$$\left. \begin{aligned} \int_V \rho \frac{\partial w^{\text{int}}}{\partial t} dV &= \frac{d}{dt} \int_V \rho w^{\text{int}} dV - \left( \rho w^{\text{int}} \frac{\partial V}{\partial t} \right) \Big|_t \\ \int_V \frac{\rho}{2} \frac{\partial u_i^2}{\partial t} dV &= \frac{d}{dt} \int_V \frac{\rho u_i^2}{2} dV - \left( \frac{\rho u_i^2}{2} \frac{\partial V}{\partial t} \right) \Big|_t \end{aligned} \right\} \quad (15)$$

Therefore (14) becomes,

$$\frac{d}{dt} \int_V \rho w^{\text{int}} + \frac{\rho u_i^2}{2} dV - \left( \rho w^{\text{int}} \frac{\partial V}{\partial t} + \frac{\rho u_i^2}{2} \frac{\partial V}{\partial t} \right) \Big|_t = \int_V \rho f_i u_i - \rho u_j \frac{\partial w^{\text{int}}}{\partial x_j} - \frac{\rho u_j}{2} \frac{\partial u_i^2}{\partial x_j} dV + \int_{\Gamma} T_i u_i d\Gamma \quad (16)$$

We can integrate (16) over time as follows,

$$\int_V \rho w^{\text{int}} + \frac{\rho u_i^2}{2} dV - \left( \rho w^{\text{int}} V + \frac{\rho u_i^2}{2} V \right) \Big|_t = \int_0^t \int_V \rho f_i u_i - \rho u_j \frac{\partial w^{\text{int}}}{\partial x_j} - \frac{\rho u_j}{2} \frac{\partial u_i^2}{\partial x_j} dV dt + \int_0^t F_i^{\text{ext}} u_i dt \quad (17)$$

By non-dimensionalising (17), we obtain,

$$\int_V \rho \bar{w}^{\text{int}} d\bar{V} + \frac{u_{\text{ref}}^2}{w_{\text{ref}}^{\text{int}}} \int_V \frac{\rho \bar{u}_i^2}{2} d\bar{V} - \left( \rho \bar{w}^{\text{int}} \bar{V} \right) \Big|_{\bar{t}} + \frac{u_{\text{ref}}^2}{w_{\text{ref}}^{\text{int}}} \left( \frac{\rho \bar{u}_i^2}{2} \bar{V} \right) \Big|_{\bar{t}} = \frac{f_{\text{ref}} u_{\text{ref}} t_{\text{ref}}}{w_{\text{ref}}^{\text{int}}} \int_0^{\bar{t}} \int_V \rho \bar{f}_i \bar{u}_i d\bar{V} d\bar{t} - \int_0^{\bar{t}} \int_V \rho \bar{u}_j \frac{\partial \bar{w}^{\text{int}}}{\partial \bar{x}_j} d\bar{V} d\bar{t} - \frac{u_{\text{ref}}^2}{w_{\text{ref}}^{\text{int}}} \int_0^{\bar{t}} \int_V \frac{\rho \bar{u}_j}{2} \frac{\partial \bar{u}_i^2}{\partial \bar{x}_j} d\bar{V} d\bar{t} + \frac{u_{\text{ref}} J_{\text{ref}}}{\rho_{\text{ref}} L_{\text{ref}}^3 w_{\text{ref}}^{\text{int}}} \int_0^{\bar{t}} \bar{F}_i^{\text{ext}} \bar{u}_i d\bar{t} \quad (18)$$

Therefore, we have the following non-dimensional coefficients from (18),

$$\frac{f_{\text{ref}} L_{\text{ref}}}{w_{\text{ref}}^{\text{int}}}; \frac{u_{\text{ref}}^2}{w_{\text{ref}}^{\text{int}}}; \frac{u_{\text{ref}} J_{\text{ref}}}{\rho_{\text{ref}} L_{\text{ref}}^3 w_{\text{ref}}^{\text{int}}} \quad (19)$$

where,

$$\bar{w}^{\text{int}} = \frac{w^{\text{int}}}{w_{\text{ref}}^{\text{int}}} \quad (20)$$

The first coefficient in (19) is analogous to Froude's number, and the second is the ratio of the kinetic energy to internal energy. The third coefficient is the ratio of the externally applied energy at the boundary to the internal energy in the domain. Again, to the best of the authors' knowledge, the second and third coefficients have never been reported in the literature. When considering two dynamically similar domains (model and prototype) with the same spatial or geometrical scale, the third coefficient can be defined as,

$$\left( \frac{\varepsilon_{ref}^{eq} F_{ref}^{ext}}{U_{ref}^{int}} \right)_{model} = \left( \frac{\varepsilon_{ref}^{eq} F_{ref}^{ext}}{U_{ref}^{int}} \right)_{prototype} \quad (21)$$

where,  $\varepsilon_{ref}^{eq}$  is the equivalent reference strain and  $U_{ref}^{int}$  is the internal reference strain energy; either  $F_{ref}^{ext}$  or  $\varepsilon_{ref}^{eq}$  can be defined for scaling the domain. The coefficients in (19) are also sufficient for achieving dynamic similitude for any given solid domain with varying material that are not strain rate sensitive and any given spatial and temporal scales, provided the continuum assumption remains valid. They also allow for the scaling of the kinematics of the two domains for both similar or different materials. For the particular case of similar material, the second coefficient in (10) enforces the same kinematics; however, the second coefficient in (19) can be used to scale the kinematics even when similar materials are used.

It should be noted that whilst the strain state of the two domains can now be variant, a new constraint emerges. For strictly accurate dynamic similarity to hold, the deformations must remain recoverable. In other words, when the strain state has been scaled between the prototype and the model, the onset of plasticity will begin to (and possibly progressively) make the two systems dissimilar. Portions of the domains undergoing unrecoverable deformation will not match, the extent of which could progressively deviate the entire solutions from dynamic similarity.

### 3 CASE STUDY – DYNAMIC STRUCTURES

In this case study, we will be considering the impact loads on a typical aircraft wing during landing. The wing geometry given by Krishnamurthy [35] is used, as shown in Figure 1, and the wing dimensions are given in Table 1. The time history of the total impact force measured by Milwitzky [36] (shown in Figure 2) for landing without tire bottoming (at the instant of ground contact), was used in this case study. The total mass of the aircraft was defined as 2,300 kg at the centre of gravity, and only a vertical landing impact is considered here. The initial vertical velocity (before impact) of 2.7 m.s<sup>-1</sup> was considered for the full-scale domain. A description of the experiment is given by Milwitzky [36]. The main landing gear is not modelled; rather, the history of the total impact force measured was applied at the location of the main landing gear.

Two different domains, which are dynamically similar, were modelled and are presented here. The wing was discretised using 127k quadrilateral four-node shell elements with full integration, and dynamic implicit analysis was conducted using the Newmark method in an in-house FE code. The material properties of both domains are given in Table 2. Domain-I is the prototype aircraft wing domain made of Aluminium Lithium alloy 2099-T8E67, and Domain-II is a 0.01 scale of Domain-I, and it is made of Aluminium alloy 2024-T351.

Table 1: Full-Scale (prototype) aircraft wing dimensions (Domain-I).

Y-location, (m)	0.00	5.461	16.8148
Chord Length, $c$ (m)	8.128	5.08	1.1514
Aerofoil Section	NACA 2414		
Leading Edge Sweep Angle, $\theta$ ( $^\circ$ )	28.4		
Single Wing Span, $b$ (m)	16.8148		
No of Ribs	26		
No. of Spars	2		

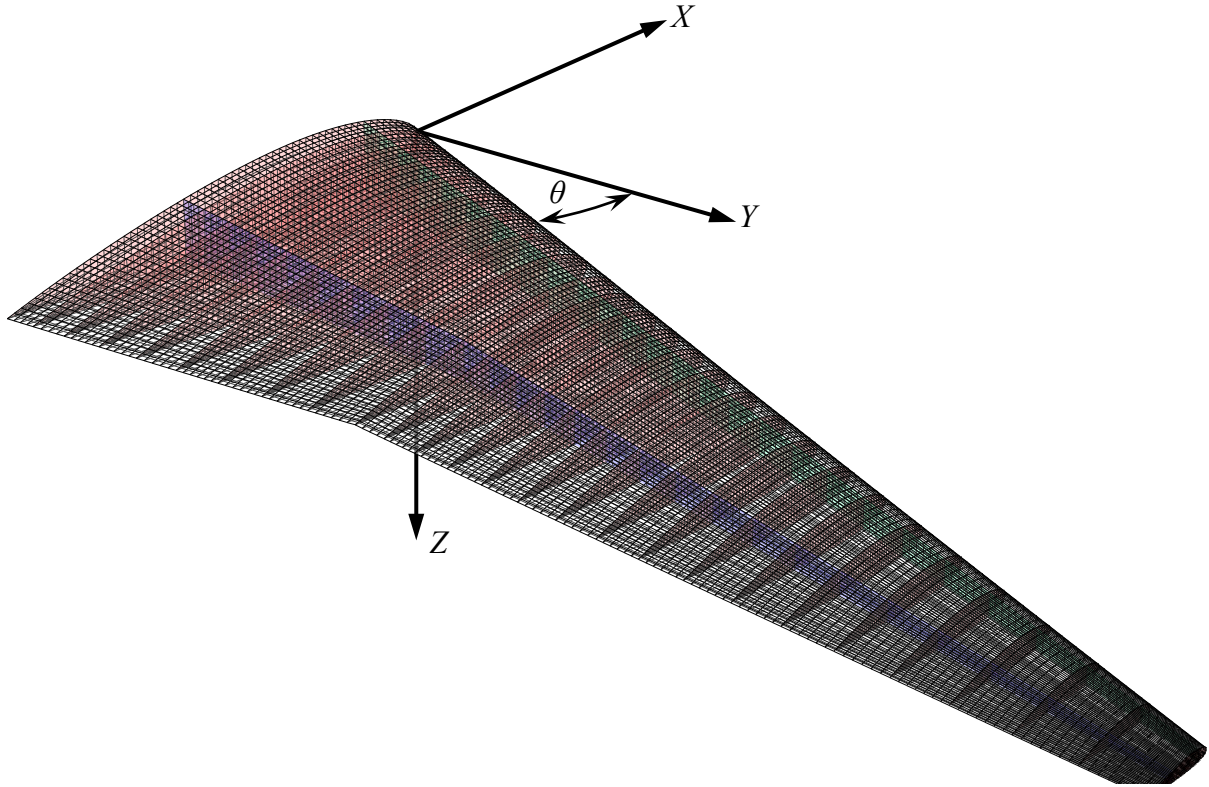


Figure 1: Typical aircraft wing.

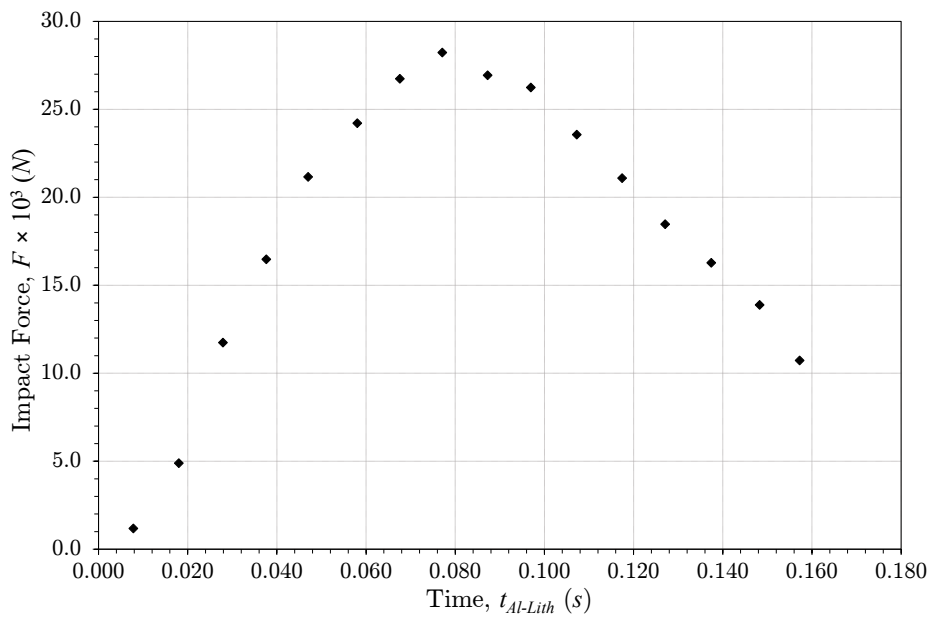


Figure 2: Impact force during landing.

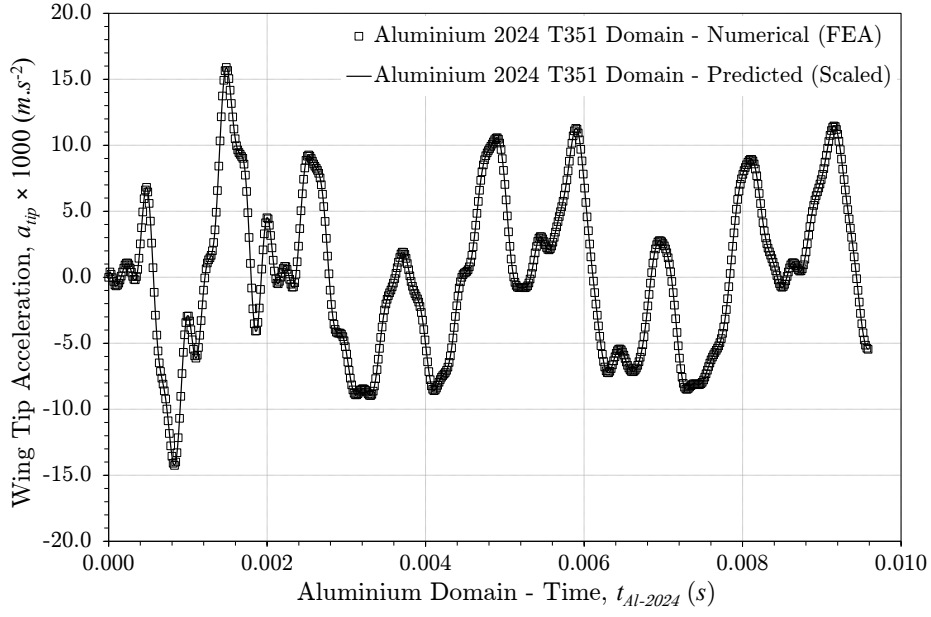


Figure 3: Comparison between the scaled wingtip acceleration and numerical results.

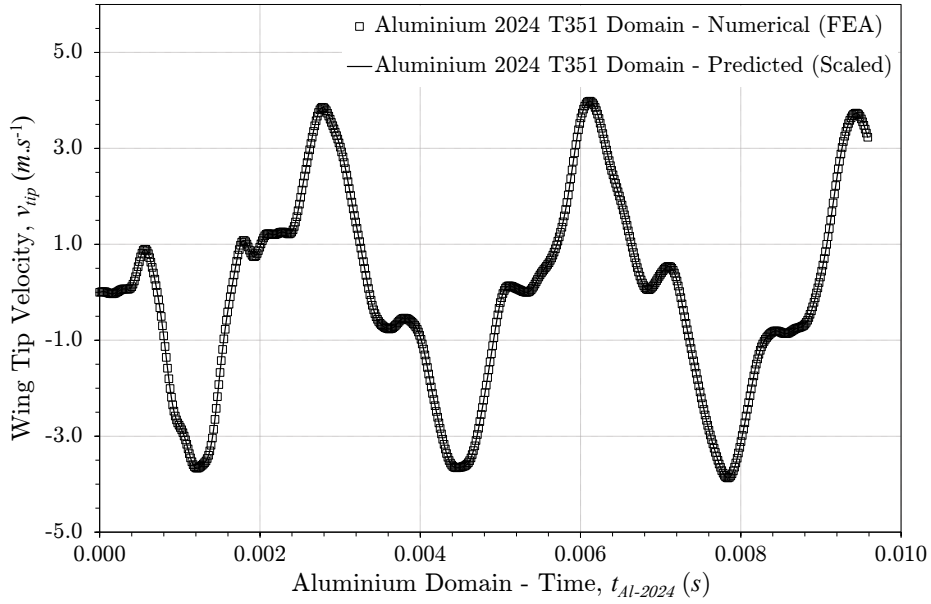


Figure 4: Comparison between the scaled wingtip velocity and numerical results.

Table 2: Domain parameters.

	Domain-I	Domain-II
Wing Material	Al-Li 2099-T8E67	Al Alloy 2024-T351
Elastic Modulus, $E$ (GPa)	78.0	72.4
Poisson's Ratio	0.35	0.33
Yield Stress, $\sigma^{yd}$ (MPa)	520	368
Density, $\rho$ (kg.m <sup>-3</sup> )	2,630.0	2,767.99
Max Force, $F_{max}$ (N)	28.228 $\times 10^3$	10.3099
Initial velocity, $v_0$ (m.s <sup>-1</sup> )	2.70	9.977
Time scale, $t$ (s)	0.9	9.5839 $\times 10^{-03}$

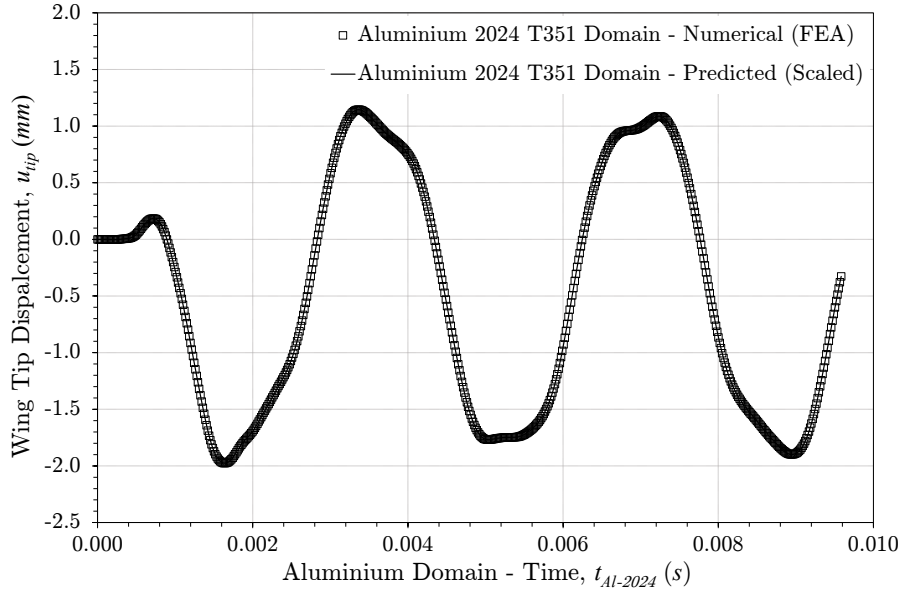


Figure 5: Comparison between the scaled wingtip displacement and numerical results.

Using the loading in Figure 2, the maximum peak of the history of equivalent strain in Domain-I occurs at the bottom edge of the root of the rear spar, and it is 4.6% of the yield strain of Aluminium Lithium alloy. For Domain-II, this equivalent strain was scaled to 23.8% of the yield strain of Aluminium alloy 2024-T351. Momentum scaling coefficients in (10) were first used to scale down the domain by a ratio of 0.01. Energy scaling coefficients in (19) were subsequently used to obtain the relevant domain parameters for the required equivalent strain in Domain-II. The resulting scaled domain parameters for Domain-II are given in Table 4.

The kinematics at the tip of the wing for the scaled model (Domain-II) is directly predicted from Domain-I. The results are compared with numerical results from the FE simulations in Figure 3 to Figure 5. The equivalent strain at the bottom edge of the root of the rear spar of Domain-I is also predicted for Domain-II and compared with FE results in Figure 6. Contour plots of the vonMises stress at equivalent time points are shown for both Domain-I and Domain-II in Figure 7. A perfect agreement is seen in all the compared results, which is to be expected as the unified scaling law developed in this paper is considered to be strictly accurate.

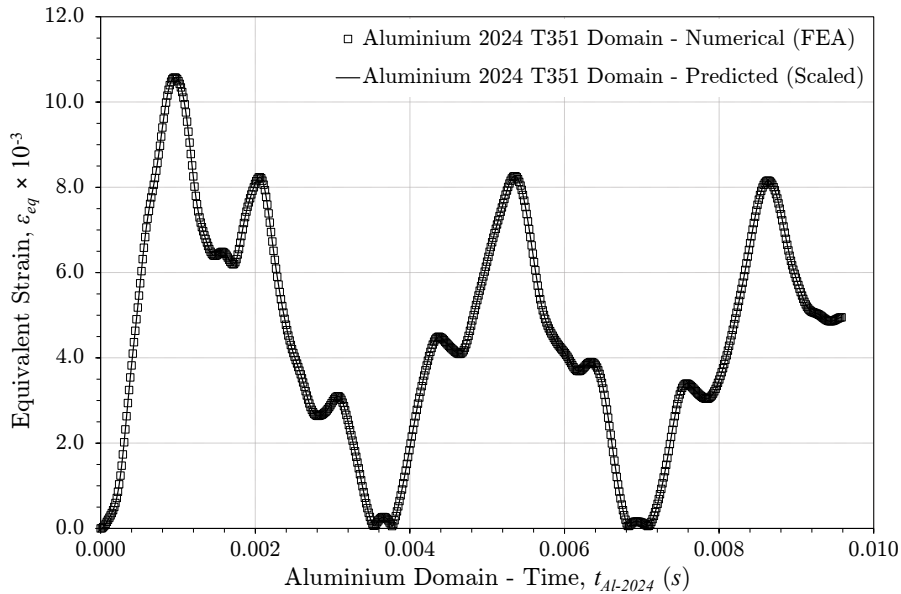


Figure 6: Comparison between the maximum equivalent strain and numerical results.

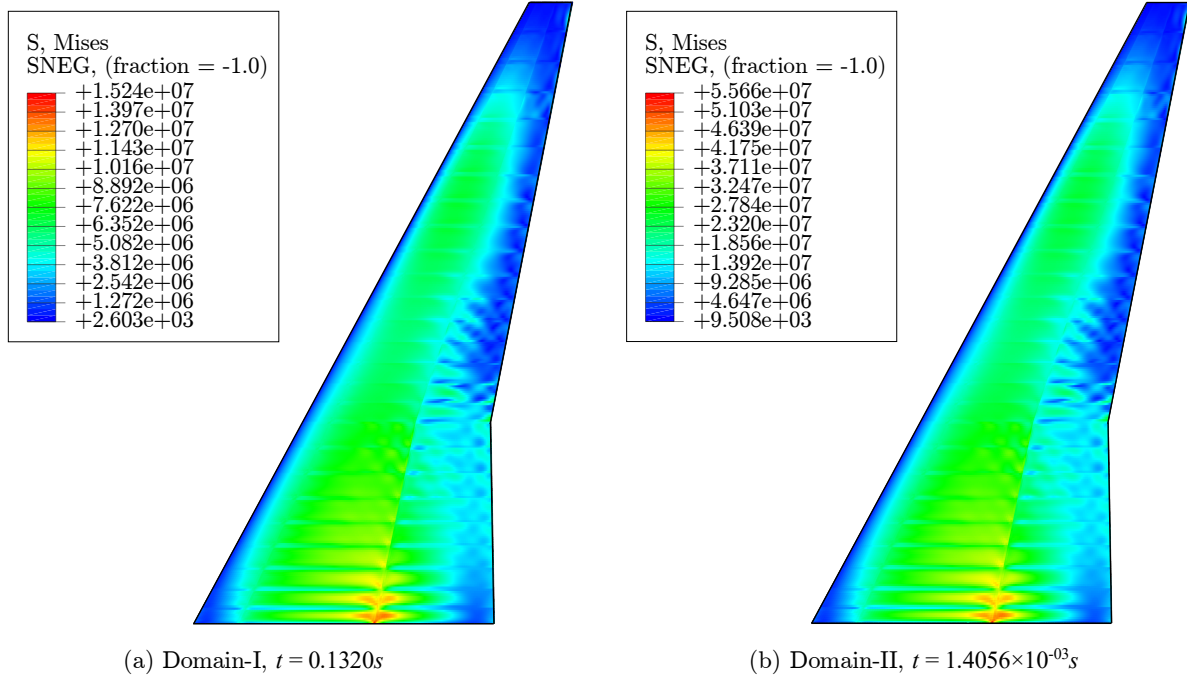


Figure 7: Comparison between the contour plots of the vonMises stress for both domains at equivalent time points.

#### 4 CASE STUDIES – AEROELASTIC STRUCTURES

In this second case study, we will be considering the exact scaling of a cantilevered flexible flat plate in a closed channel. The domain is shown in Figure 8, and the flat plate is clamped at one end. The channel dimensions are chosen to ensure a fully developed flow and that the boundary conditions do not affect the computed flow. The plate is with an incidence of  $\alpha_0 = 2.5^\circ$ .

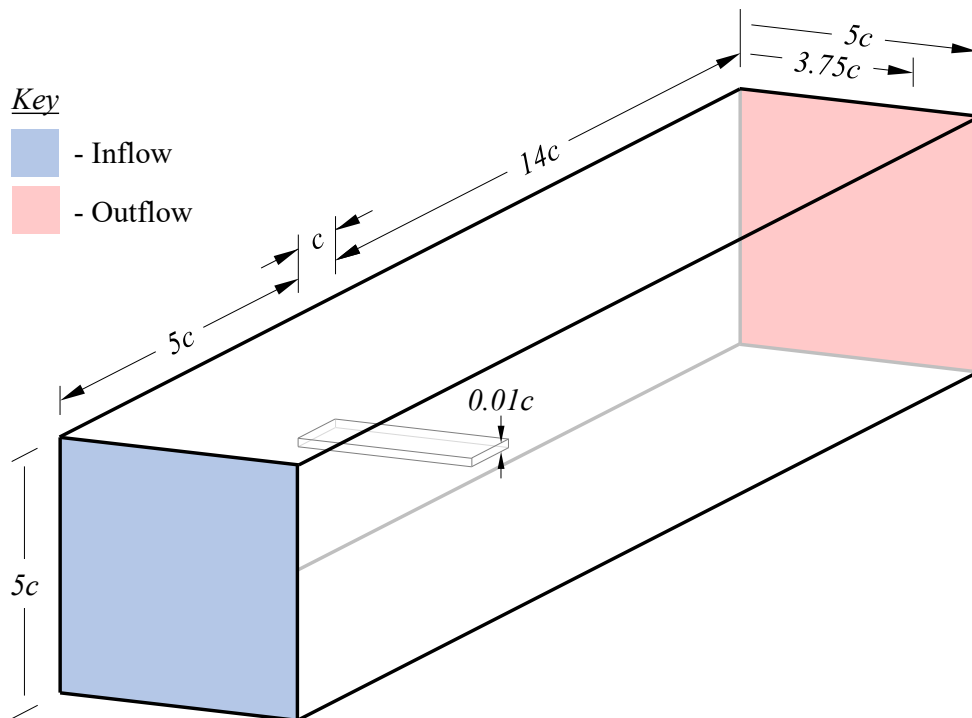


Figure 8: Schematic of fluid domain (not to scale).

Table 3: Full-Scale (prototype) and scaled (model) material properties and boundary conditions.

	Domain-III	Domain-IV
Elastic Modulus, $E$ (GPa)	3.3	586.67
Poisson's Ratio	0.35	0.35
Plate Density, $\rho_s$ (kg.m <sup>-3</sup> )	1180.0	1180.0
Initial velocity, $v_0$ (m.s <sup>-1</sup> )	2.5	33.333
Time scale, $t$ (s)	0.75	$4.219 \times 10^{-03}$
Flow Density, $\rho_a$ (kg.m <sup>-3</sup> )	1.224	1.224
Freestream Temperature, $T_0$ (K)	290.372	290.372
Reynolds Number, Re	$1.70 \times 10^5$	$1.70 \times 10^5$
Max Total Lift Force, $L_{max}$ (N)	3.038	3.043

Two domains, which share dynamics similitude, were modelled and are presented here. The domain was discretised with 1.5 million cells as shown in Figure 9. The Mach number for prototype domain is 0.007 while for the model is 0.098, hence the flow is effectively incompressible. The simulations were conducted using the commercial code Fluent; for the fluid continuum, solving the Unsteady Reynolds Average Navier Stokes (URANS) equations using finite volume method and for the solid continuum, finite element method is used. For turbulence modelling, especially at flow separation, the  $k - \omega$  with shear stress transport (SST) model was used. A regular hexahedral mesh was used for discretisation as shown in Figure 9. A maximum values of  $y^+ > 1$  is ensured for the mesh near the plate wall. The gradients are computed with a cell based least squares method and for transient simulations, second order time discretisation is used. Steady state simulations were initially conducted and the results were validated using lift distribution from circulation distribution calculated from Prandtl's equation for a rectangular wing. For modelling transient effects, the CLF number was kept below 1 everywhere in the domain, hence time step of  $1 \times 10^{-4}$  s was adopted.

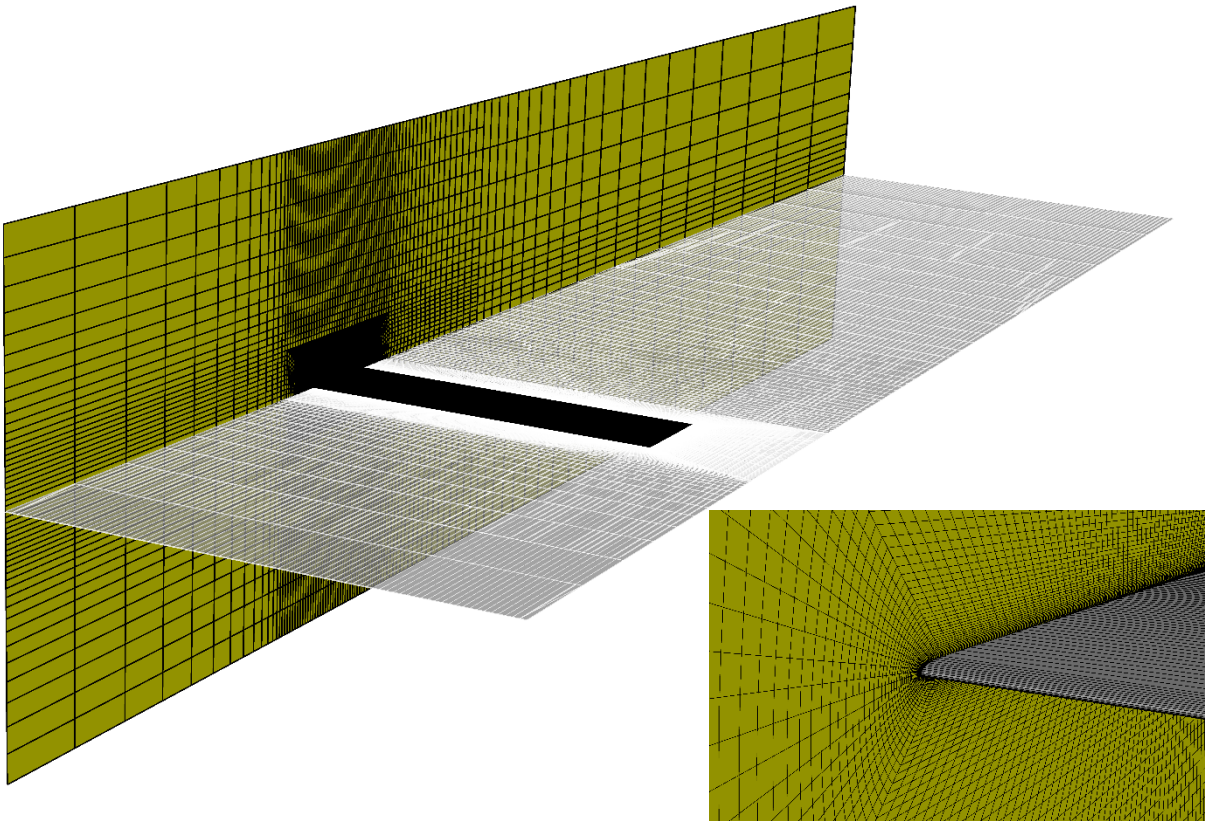


Figure 9: Discretised fluid domain.

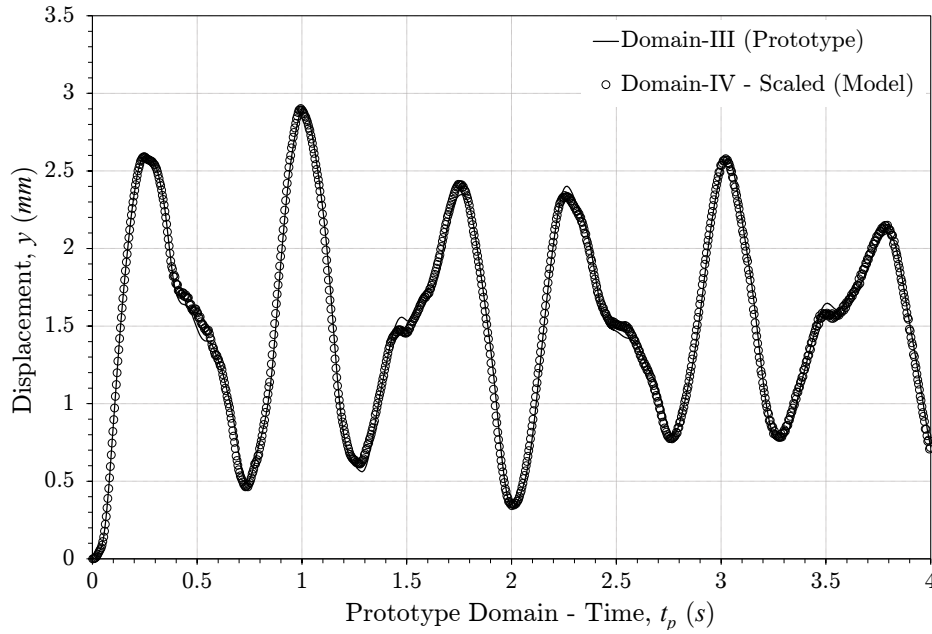


Figure 10: Comparison between the scaled leading edge wingtip displacement and numerical results.

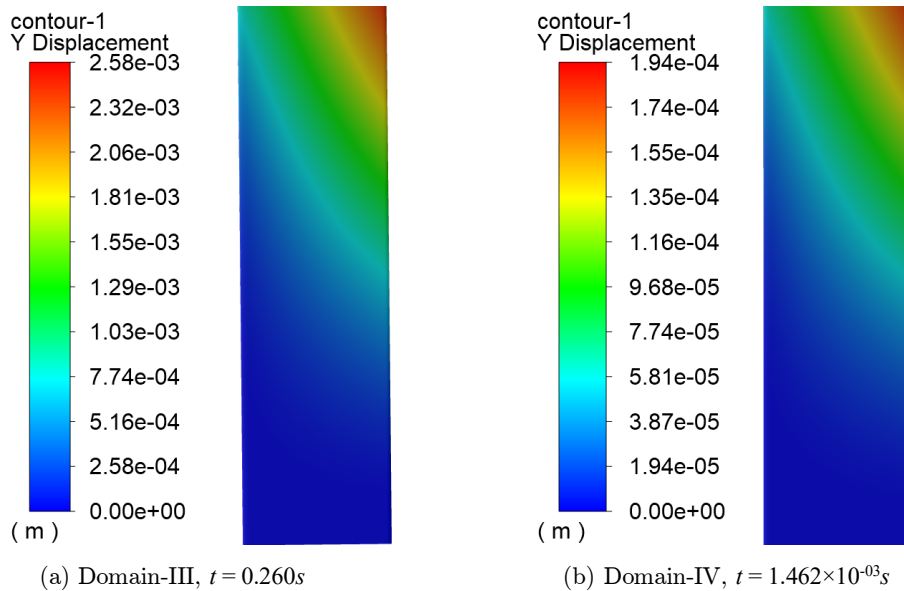


Figure 11: Comparison between the contour plots of the  $y$ -displacement for both domains at equivalent time points.

For the solid domain, the Newmark method was again adopted for time integration when solving the finite element semi-discrete equation of motion. For considering geometric non-linearity, the reference configuration is based on initial configuration and quantities are formulated using total Lagrangian formulation. The material properties of both domains are given in Table 3.

Domain-III is the prototype domain and Domain-IV is a 0.075 scale of Domain-III. The momentum scaling coefficients were used to scale down the domain in this case study. The kinematics at the leading edge tip of the flat plate for the prototype (Domain-III) is directly predicted from Domain-IV. The scaled results are compared to results from Domain III in Figure 10. Contour plots of the normal displacement of the plate at equivalent time points are

shown for Domain-III and Domain-IV in Figure 11. A very good agreement is seen in all the compared results, which confirms dynamic similitude.

## 5 CONCLUDING REMARKS

Coupled with the drive for efficient aircraft wing through high aspect ratio wing is the growing need for much more accurate aeroelastic analyses of aircraft wings and there is the need for more accurate experimental tests at both design and certification stages of new structures and a unified model that achieves dynamic similitude in aeroelastic structures.

In this article we presented a unified approach for scaling solid continuum using non-dimensional coefficients obtained from the momentum and energy conservation and its application in dynamic and aeroelastic structures. Whilst some of the numbers are analogous to existing numbers, others have never been reported in the literature. Two case studies were considered: the scaling of an aircraft wing experiencing dynamic landing impact loads and the scaling of an aeroelastic structure under aerodynamic loads. The dynamically similar solutions are strictly accurate across all spatial and temporal scales of the continuum, and this is clearly seen in the very good agreement observed in all the results presented in the case studies.

## 6 ACKNOWLEDGEMENTS

We are grateful to the UK Materials and Molecular Modelling Hub for computational resources, which is partially funded by EPSRC (EP/P020194/1 and EP/T022213/1).

## 7 REFERENCES

- [1] Cooper, J., Lind, R. and Wright, J. (2010). Aeroelastic Testing and Certification. Encyclopedia of Aerospace Engineering, edited by Blockley, Richard, and Shyy, Wei, John Wiley and Sons Ltd., West Sussex, 3, 1641–1651, Chap. 138.
- [2] Newton, I. (1687). *Philosophiae naturalis principia mathematica*. William Dawson & Sons Ltd, London.
- [3] Stokes, G.G. (1850). On the effect of the internal friction of fluids on the motion of pendulums. *Trans. Cambridge Philos.*, 9, 8-106.
- [4] Reynolds, O. (1883). An experimental investigation of the circumstances which determine whether the motion of water shall be direct or sinuous, and of the law of resistance in parallel channels. *Phil. Trans. R. Soc.*, 174, 935-982.
- [5] Rayleigh L. (1915). The principle of similitude. *Nature*, 95, 66-68.
- [6] Goodier, J.N. and Thomson, W.T. (1944). Applicability of similarity principles to structural models. Technical Report TN-933, NACA.
- [7] Mixson, J.S. and Catherine, J.J. (1964). Experimental lateral vibration characteristics of a 1/5-scale model of Saturn SA-1 with an eight-cable suspension system. Technical Report TN-D-2214, NASA.
- [8] Canfield S.L., Peddieson J. and Garbe G. (2010). Similarity rules for scaling solar sail systems. Technical Report M10-0055, NASA.
- [9] Baker, W.E. (1978). Scaling and prediction of impact puncture of shipping casks for radioactive materials. *Shock Vibr. Bull.*, 48, 143.
- [10] Vassalos D. (1999). Physical modeling and similitude of marine structures. *Ocean Eng.*, 26, 111–23.
- [11] Wen, H.-M. and Jones, N. (1993). Experimental Investigation of the Scaling Laws for Metal Plates Struck by Large Masses. *Int. J. Impact. Engng.*, 13(3), 485-505.

- [12] Simitzes, G.J. and Rezaeepazhand, J. (1993). Structural Similitude for Laminated Structures. *Composite Engng.*, 3(7-8), 751-765.
- [13] Wu J.J., Cartmell M.P. and Whittaker A.R. (2002). Prediction of the vibration characteristics of a full-size structure from those of a scale model. *Comput Struct.*, 80(18-19), 1461–1472.
- [14] Jackson K.E., Fasanella E.L. and Lyle K.H. (2003). Comparisons of the impact responses of a 1/5-scale model and a full scale crashworthy composite fuselage section. American helicopter society 59th annual forum, Phoenix, AZ.
- [15] Macagno, E.O. (1971). Historico-critical review of dimensional analysis. *J. Franklin Inst.*, 292, 391-402.
- [16] Simitzes G.J., Starnes J. and Rezaeepazhand J. (2001). Structural similitude and scaling laws for plates and shells: A Review. *Advances in the Mechanics of Plates and Shells. Solid Mechanics and its Applications - Book Series 88*, Springer, Dordrecht.
- [17] Coutinho, C.P., Baptista, A.J. and Rodrigues, J.D. (2016). Reduced scale models based on similitude theory: a review up to 2015. *Engineering Structures*, 119, 81-94.
- [18] Casaburo, A., Petrone, G., Franco, F. and De Rosa, S. (2019). A Review of similitude methods for structural engineering. *ASME. Appl. Mech. Rev.*, 71, 030802.
- [19] Bisplinghoff, R.L. and Ashley, H. (1962). *Principles of Aeroelasticity*. New York: Wiley & Sons.
- [20] Friedmann, P.P., Guillot, D. and Presente, E. (1997). Adaptive Control of Aeroelastic Instabilities in Transonic Flow and Its Scaling. *Journal of Guidance, Control, and Dynamics*, 20(6), 1190–1199.
- [21] Friedmann, P.P. and Presente, E. (2001). Active Control of Flutter in Compressible Flow and its Aeroelastic Scaling. *Journal of Guidance, Control, and Dynamics*, 24(1), 167–175.
- [22] Pototzky, A.S. (2002). Scaling Laws Applied to a Modal Formulation of the Aeroservoelastic Equations. AIAA 2002-1598. 43rd AIAA/ASME/ASCE/AHS/ASC Structures, Structural Dynamics, and Materials Conference. April 2002.
- [23] Wan, Z., Cesnik, C.E.S. (2014). Geometrically non-linear aeroelastic scaling for very flexible aircraft. *AIAA Journal*, 52(10), 2251–2260.
- [24] French, M. and Eastep, F.E. (1996). Aeroelastic Model Design Using Parameter Identification. *Journal of Aircraft*, 33(1), 198–202.
- [25] Bond, V.L., Canfield, R.A., Suleman, A. and Blair, M. (2012). Aeroelastic Scaling of a Joined Wing for Nonlinear Geometric Stiffness. *AIAA Journal*, 50(3), 513–522.
- [26] Ricciardi, A.P., Eger, C.A.G., Canfield, R. A., Patil, M. J. and Lindsley, N. (2012). High Fidelity Nonlinear Aeroelastic Analysis for Scaled Vehicle Design. AIAA 2012-5624. 12th AIAA Aviation Technology, Integration, and Operations (ATIO) Conference and 14th AIAA/ISSMO Multidisciplinary Analysis and Optimization Conference. September 2012.
- [27] Georgiou, G., Vio, G.A. and Cooper, J.E. (2014). Aeroelastic tailoring and scaling using Bacterial Foraging Optimisation. *Structural and Multidisciplinary Optimisation*, 50, 81–99.
- [28] Afonso, F., Vale, J., Oliveira, E., Lau, F. and Suleman, A. (2017). A review on non-linear aeroelasticity of high aspect-ratio wings. *Progress in Aerospace Sciences*, 89, 40-57.
- [29] Buckingham, E. (1914). On Physically Similar Systems: Illustrations of the Use of Dimensional Equations. *Phys. Rev.*, 4, 345-376.

- [30] Li, L., Luo, Z., He, F., Zhao, X. and Liu, J. (2020). A partial similitude method considering variable powers in scaling laws and applied to rotor-bearing systems. *Int. J. Mech. Sci.*, 186, 105892.
- [31] El-Borgi, S., Alrumaihi, A., Rajendran, P., Yazbeck, R., Fernandes, R., Boyd, J.G., Lagoudas, D.C. (2021). Model updating of a scaled piping system and vibration attenuation via locally resonant bandgap formation. *Int. J. Mech. Sci.*, 194, 106211.
- [32] Afonso, F., Coelho, F., Vale, J., Lau, F. and Suleman, A. (2020). On the Design of Aeroelastically Scaled Models of High Aspect-Ratio Wings. *Aerospace*, 7(11), 166.
- [33] Adetoro, O.B. and Cardoso, R.P.R. (2021). On the Mechanical Dynamic Similitude of Solid Continuum. *International Journal of Impact Engineering*, 154, 103876.
- [34] Johnson, W. (1972). *Impact Strength of Materials*. Edward Arnold, London.
- [35] Krishnamurthy, T. and Tsai, F.J. (2008). Static and Dynamic Structural Response of an Aircraft Wing with Damage Using Equivalent Plate Analysis. 49th AIAA/ASME/ASCE/AHS/ ASC Structures, Structural Dynamics, and Material Conference, 7-10 April 2008, Schaumburg, IL.
- [36] Milwitzky, B., Cook, F.E. (1953). Analysis of Landing-gear Behavior. NACA, Washington, DC, Technical Report TR-1154, NACA.

#### **COPYRIGHT STATEMENT**

The authors confirm that they, and/or their company or organisation, hold copyright on all of the original material included in this paper. The authors also confirm that they have obtained permission, from the copyright holder of any third party material included in this paper, to publish it as part of their paper. The authors confirm that they give permission, or have obtained permission from the copyright holder of this paper, for the publication and distribution of this paper as part of the IFASD-2022 proceedings or as individual off-prints from the proceedings.